Journal of Physics: Conference Series **489** (2014) 012037 doi:10.1088/1742-6596/489/1/012037

2D-3D registration for brain radiation therapy using a 3D CBCT and a single limited field-of-view 2D kV radiograph

R Munbodh[1], **D J Moseley**[2]

[1] Department of Radiation Oncology, University of Pennsylvania, Philadelphia, PA, USA
[2] Radiation Medicine Program, Princess Margaret Hospital, Toronto, Canada

E-mail: Reshma.Munbodh@uphs.upenn.edu

Abstract. We report results of an intensity-based 2D-3D rigid registration framework for patient positioning and monitoring during brain radiotherapy. We evaluated two intensity-based similarity measures, the Pearson Correlation Coefficient (ICC) and Maximum Likelihood with Gaussian noise (MLG) derived from the statistics of transmission images. A useful image frequency band was identified from the bone-to-no-bone ratio. Validation was performed on gold-standard data consisting of 3D kV CBCT scans and 2D kV radiographs of an anthropomorphic head phantom acquired at 23 different poses with parameter variations along six degrees of freedom. At each pose, a single limited field of view kV radiograph was registered to the reference CBCT. The ground truth was determined from markers affixed to the phantom and visible in the CBCT images. The mean (and standard deviation) of the absolute errors in recovering each of the six transformation parameters along the x, y and z axes for ICC were ϕ_x: 0.08(0.04)°, ϕ_y: 0.10(0.09) °, ϕ_z: 0.03(0.03)°, t_x: 0.13(0.11) mm, t_y: 0.08(0.06) mm and t_z: 0.44(0.23) mm. For MLG, the corresponding results were ϕ_x: 0.10(0.04)°, ϕ_y: 0.10(0.09)°, ϕ_z: 0.05(0.07)°, t_x: 0.11(0.13) mm, t_y: 0.05(0.05) mm and t_z: 0.44(0.31) mm. It is feasible to accurately estimate all six transformation parameters from a 3D CBCT of the head and a single 2D kV radiograph within an intensity-based registration framework that incorporates the physics of transmission images.

1. Introduction

In the treatment of brain tumours with photon or proton radiation, accurate radiation delivery is critical for local tumour control and the sparing of healthy tissue. We have previously developed an automated 2D-3D rigid registration framework for patient positioning during prostate radiotherapy [1–5]. In this study, we extend our previous methods and develop an automated, accurate image-guided solution specific to radiation therapy of intracranial and skull base tumours. Patient setup errors are determined by registering 2D kV radiographs acquired during a particular treatment fraction to a 3D CBCT, which provides the desired position of the patient with respect to the treatment beams. By providing a framework for improved patient setup and, as a result, reduced geometrical (targeting) uncertainties in the delivery of the radiation with minimal additional imaging dose, we expect reduced radiation-induced toxicity while maintaining similar treatment outcomes. We will validate two similarity measures, the Pearson correlation coefficient and the maximum likelihood measure with Gaussian noise. These

similarity measures make different assumptions about the nature of signal and noise in the CBCT images and 2D radiographs.

2. Methods

2.1. Pose determination experiments

Validation was performed on gold-standard data consisting of 3D kV CBCT scans and 2D kV radiographs of an anthropomorphic head phantom acquired on a robotic couch at each of 23 known poses with parameter variations along all six degrees of freedom (translations of up to 10 mm and rotations of up to 3.5°). The ground truth at each pose was determined by registering radio-opaque ball bearings affixed to the phantom and visible in the CBCT images to ball bearings in the reference CBCT. We used single, limited field-of-view (FOV) 2D kV radiographs ($\sim 10\times10$ cm^2 of the 17×20 cm^2 phantom head size, resolution: 1 mm^2) in the anterior-posterior view comprising the orbits and part of the nasal structures for registration to the reference 3D CBCT (resolution: 1 mm^3). Limited FOV kV radiographs permit reduced imaging dose and also ensure exclusion of any patient immobilisation devices from the registration. The x-axis was directed across the subject from right to left, the y-axis along the subject from toe to head and the z-axis through the subject towards the x-ray source. In-plane parameters were t_x, t_y and ϕ_z and out-of-plane parameters were ϕ_x, ϕ_y and t_z.

2.2. Similarity measures

Given a 3D kV CBCT and a 2D kV radiograph, our task, is to estimate the global rigid tranformation, ψ, which aligns the CBCT to the 2D radiograph. The transformation ψ is a vector consisting of three translations, t_x, t_y and t_z, and three rotations, ϕ_x, ϕ_y and ϕ_z, around the x, y and z axes. The optimal transformation, ψ, was found by iteratively shifting and rotating the CBCT until the similarity between the DRR, $\mathbf{v}_\psi$, which is a perspective projection of the CBCT at transformation ψ and the 2D radiograph, $\mathbf{u}$, was maximised. In this study, we evaluated two intensity-based similarity measures, the Pearson correlation coefficient (ICC) and the maximum likelihood measure with Gaussian noise (MLG) [5]. ICC measures the strength of the linear relationship between two normal random variables. MLG assumes that Poisson noise is a limiting source of noise in the 2D kV radiographs and for a large number of photons, the Poisson noise can be approximated by non-stationary Gaussian noise. It assumes that the pixel intensities in the 2D kV radiograph are obtained from a non-stationary Gaussian process with mean and variance given by the intensity values of the corresponding pixels in the 2D DRR. Previously, we showed that high-pass filtering the DRRs and radiographs reduced the bias and variance in the registration results [3]. Here, the cutoff frequency for the filter was determined from the bone-to-no-bone ratio projection images of a CT of the head phantom.

2.3. Quantification of registration error

In addition to examining the errors in the individual transformation parameters at every pose, we computed the final target registration error (TRE) as the mean distance, $\mathcal{E} = \frac{1}{n}\sum_{i=1}^{n}\|(T_{\hat{\psi}} - T_\psi)x_i\|$, moved by n uniformly distributed points on a virtual sphere of radius 3 cm centred at the simulated isocentre, and representing the tumour, from their intended position. $T_{\hat{\psi}}$ and T_ψ are the transformation matrices at the estimated and actual transformation parameters, respectively, and x are the 3D coordinates of the points on the surface of the sphere. We examined the final TRE as a function of initial TRE defined as $\mathcal{E}_o = \frac{1}{n}\sum_{i=1}^{n}\|T_\psi x_i\|$.

3. Results

Fig. 1(a) shows the final TRE, $\mathcal{E}$, as a function of the initial TRE, $\mathcal{E}_o$ for each of the 14 poses with translational shifts only for the two similarity measures. A single 2D kV radiograph in

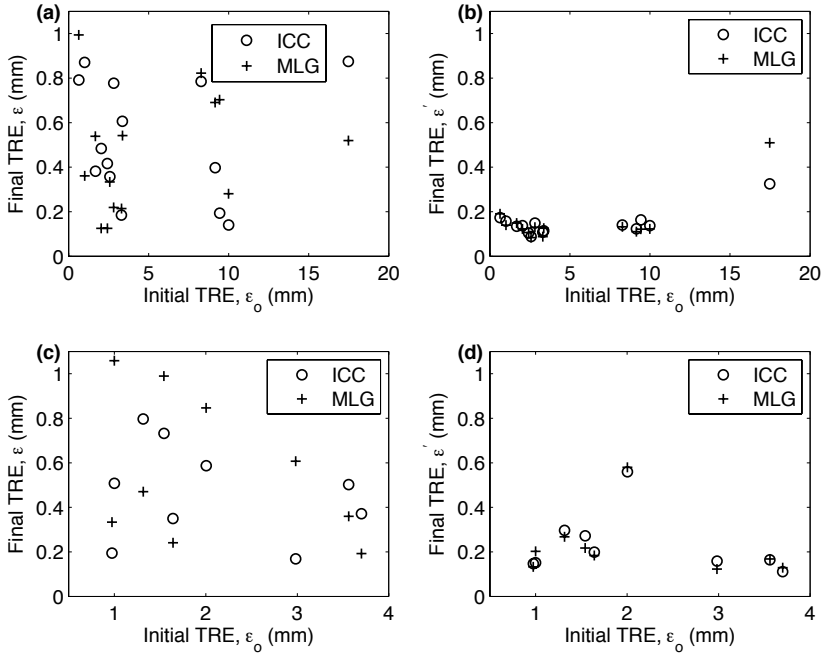

Figure 1. Final TRE as a function of initial TRE. The final TRE, $\mathcal{E}$, due to errors in estimating the six transformation parameters is shown in (a) and the final TRE, $\mathcal{E}'$, excluding the error in estimating t_z, is shown in (b) for poses with translational displacements only. (b) and (c) show $\mathcal{E}$ and $\mathcal{E}'$, respectively, for poses with rotations or combinations of rotations and translations.

the AP view was used for the registration. The initial TRE ranged from 0.63 mm to 17.5 mm. The final TRE was less than 1 mm for all 14 poses for both ICC and MLG. Even though the out-of-plane translation, t_z, was solved to better than 1 mm in all instances, errors in estimating t_z were the largest contributor to the overall registration error. Fig. 1 (b) shows the final TRE excluding errors in estimating t_z. The final TRE, $\mathcal{E}'$, in this case was smaller than 0.2 mm for 13 of the 14 poses. Figs. 1 (c) and (d) show similar plots for the nine poses that had either rotations only or combinations of rotations and translations of 3 mm along each axis. Once again, errors in estimating t_z were the largest as illustrated in the reduction in the final TRE in Fig. 1 (d). The presence of in-plane and out-of-plane rotations did not seem to adversely affect the performance of the registration algorithm. The magnitude of the final TRE for both the translational and rotational poses was not correlated to the magnitude of the initial TRE.

A box plot of the distribution of absolute errors in estimating each of the six transformation parameters and the final target registration errors, $\mathcal{E}$ and $\mathcal{E}'$,is shown in Fig. 2. The lines in the boxes denote the lower quartile, median and upper quartile values. The mean (and standard deviation) of the absolute errors in recovering each of the six transformation parameters along the x, y and z axes for ICC were ϕ_x: 0.08(0.04)°, ϕ_y: 0.10(0.09)°, ϕ_z: 0.03(0.03)°, t_x: 0.13(0.11) mm, t_y: 0.08(0.06) mm and t_z: 0.44(0.23) mm. For MLG, the corresponding results were ϕ_x: 0.10(0.04)°, ϕ_y: 0.10(0.09)°, ϕ_z: 0.05(0.07)°, t_x: 0.11(0.13) mm, t_y: 0.05(0.05) mm and t_z: 0.44(0.31) mm.

4. Discussion

The performance of ICC and MLG was found to be comparable. In-plane and out-of-plane parameters were estimated to better than 1 mm and 1° accuracy with both similarity measures, as quantified by the mean of the absolute registration error. Estimates of the out-of-plane translation, t_z, had the largest uncertainty. This is attributable to the imaging geometry. The results suggest that an accuracy of better than 0.5 mm can be obtained by using a second radiograph in the lateral view for the registration and where t_z would be an in-plane translation.

Most registration methods for setup verification are 2D and semi-automated. Semi-automated 2D-3D methods for the skull include [6]. Automated 2D-3D registration methods for

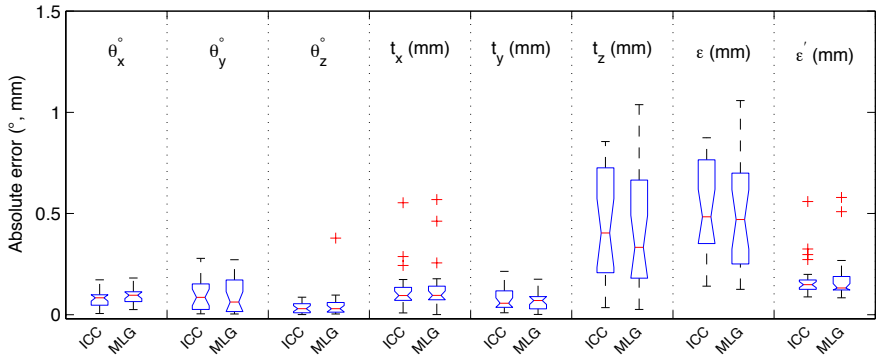

Figure 2. Box plot showing the distribution of absolute errors in estimating the six transformation parameters and the final target registration errors, $\mathcal{E}$ and $\mathcal{E}'$.

radiotherapy are few and employ two orthogonal 2D radiographs. They include intensity-based methods using pattern intensity [7], stochastic rank correlation [8], correlation-based measures and information theoretic measures [9–12]. Feature-based methods include [13–15], and hybrid methods include [16]. Automated 2D-3D methods applied to brain RT include an intensity-based method [17] and gradient-based approaches [18, 19]. The testing performed and results achieved in this study with a single 2D radiograph compare favourably with the above studies.

Our results suggest that at current imaging doses and levels of Poisson noise in 2D radiographs of the head, ICC and MLG are equivalent. The MLG method provides insight as to why ICC would work for these images. For larger levels of noise and lower images doses, we might expect MLG to provide better registration accuracy. Results from our study support the importance of understanding the image formation process and of modelling the relationship between intensity values in the two modalities to guide the choice of similarity measure in intensity-based registration of CT to x-ray images.

5. Conclusions

We have presented an automated 2D-3D registration framework for patient setup during brain radiation therapy. Sub-millimeter registration accuracy was obtained with two similarity measures and a single, limited FOV 2D kV radiograph.

References

[1] Munbodh R 2004 *Achieving accurate automated image registration for prostate radiotherapy* Ph.D. thesis Yale University
[2] Munbodh R, Jaffray D A, Moseley D J *et al.* 2006 *Med. Phys.* **33** 1398–1411
[3] Munbodh R, Chen Z, Jaffray D A *et al.* 2007 *Med. Phys.* **34** 3005–3017
[4] Munbodh R, Chen Z, Jaffray D *et al.* 2008 *Med. Phys.* **35** 4352–4361
[5] Munbodh R, Tagare H, Chen Z *et al.* 2009 *Med. Phys.* **36** 4555–4568
[6] Lujan A E, Balter J M and Ten Haken R K 1998 *Med. Phys.* **25** 703–8
[7] Penney G P, Batchelor P G, Hill D L *et al.* 2001 *Med. Phys.* **28** 1024–1032
[8] Birkfellner W, Stock M, Figl M *et al.* 2009 *Med. Phys.* **36** 3420–3428
[9] Penney G P, Weese J, Little J A *et al.* 1998 *IEEE Trans. on Medical Imaging* **17** 586–595
[10] Kim J, Fessler J A, Lam K L *et al.* 2001 *Med. Phys.* **28** 2507–2517
[11] Clippe S, Sarrut D, Malet C *et al.* 2003 *Int. J. Radiat. Oncol. Biol. Phys.* **56** 259–265
[12] Kim J and Fessler J A 2004 *IEEE Trans. Medical Imaging* **23** 1430–1444
[13] Tomaževič D, Likar B, T S and Pernuš F 2003 *IEEE Trans. Medical Imaging* **22** 1407–1416
[14] Livyatan H, Yaniv Z and Joskwicz L 2003 *IEEE Trans. Medical Imaging* **22** 1395–1406
[15] Gilhuijs K G, van de Ven P and van Herk M 1996 *Med. Phys.* **23** 389–399 PMID: 8815382
[16] Bansal R, Staib L H, Chen Z *et al.* 2003 *IEEE Trans. Medical Imaging* **22** 29–49
[17] Fu D, Kuduvalli G, Mitrovic V *et al.* 2005 *SPIE* **5744** 1605–7422
[18] Lemieux L, Jagoe R, Fish D R *et al.* 1994 *Med. Phys.* **21** 1749–1760
[19] Murphy M J 1997 *Med. Phys.* **24** 857–866